JOINT INVERSION OF GRAVITY AND GROUND PENETRATING RADAR DATA TO CHARACTERIZE SUBSURFACE CAVITIES

BY

FATHI MOHAMMED SAEED ABDULLAH

A Thesis Presented to the

DEANSHIP OF GRADUATE STUDIES

KING FAHD UNIVERSITY OF PETROLEUM & MINERALS

DHAHRAN, SAUDI ARABIA

In Partial Fulfillment of the
Requirements for the Degree of

MASTER OF SCIENCE

In

GEOPHYSICS

MAY, 2014

KING FAHD UNIVERSITY OF PETROLEUM & MINERALS
DHAHRAN 31261, SAUDI ARABIA

DEANSHIP OF GRADUATE STUDIES

This thesis, written by **Fathi Mohammed Saeed Abdullah** under the direction of his thesis advisor and approved by his thesis committee, has been presented to and accepted by the Dean of Graduate Studies, in partial fulfillment of the requirements for the degree of
MASTER OF SCIENCE IN GEOPHYSICS.

Thesis Committee

Dr. Abdullatif A. Al-Shuhail (Advisor)

Dr. SanLinn Ismail Kaka (Member)

Dr. Khalid Al-Ramadan (Member)

Dr. Abdulaziz Al-Shaibani
(Department Chairman)

Dr. Salam A. Zummo
(Dean of Graduate Studies)

21/5/14

Date:

©Fathi Mohammed Saeed Abdullah

2014

Dedicated

To the memory of my father, who guided me through the wilderness of this life.

To my mother, whom I owe my life.

To my remarkable wife and my wonderful daughter Rawah who sustains my life in every way and to their patience during the progress of this work.

ACKNOWLEDGEMENTS

First of all, Praise is to Allah, the Lord of the worlds, who gave me the blessing of health and wellness to accomplish this work. Then, I would like to express my gratitude to all people who helped and encouraged me to finish this thesis.

I am deeply indebted to my supervisor Dr. Abdullatif Al-Shuhail for his insightful advice and suggestions, continuous motivation and most of all patience throughout the entire work. I have learned a lot from him through this work, especially in scientific thinking and problem solving.

I would like to extend my great appreciation to my committee members, Dr. SanLinn Ismail Kaka for his encouragement during the progress of the work and for Dr. Khalid Al-Ramadan for his attention and moral support.

I wish to express my sincere thanks to the Earth Science Departement at KFUPM and the Chairman Dr. Abdulaziz Al-Shaibani for his help, encouragement and facilities during the work.

I would like to express my profound gratitude to Dr. Amin Noman Al-

Kadasi for giving me generous amount of time whenever it is needed and for his moral support. He was the first who inspire me to think as a geophysical researcher.

Also I express special thanks for all Geology Department faculty and staff at Taiz University for their attention and constant support.

I am also thankful to Prof. Dr. Hosni Ghazala, Geology Department, Mansoura University, Egypt, for his constant encouragement and moral support.

I feel grateful to all my friends in KFUPM for being in contact with me and encouraging me. My deep thanks goes to my close friend Hasan Alshehab for being very helping and cooperative.

My great appreciation go to all of my family members especially to my eldest brothers Abdulhakeem and Gharsan for their relentless support and encouragement in helping me fulfill this aspiration and without their support and guidance I would not be where I am today.

My sincere thanks are due to the Taiz University for the financial support during this work and my deep thanks to KFUPM which provided me all the facilities through my study.

Finally, the warm love and affection for my lovely wife Sahar and my daughter Rawah, for their prayer to finish this work, are deeply thankful.

Contents

List of Tables

List of Figures

ABBREVIATIONS AND SYMBOLS

EM	Electromagnetic
GPR	Ground Penetrating Radar
H_s	Thickness of host layer
H_{s1}	Distance from ground surface to top of cavity
H_{s2}	Distance from bottom of cavity to bottom of host layer
H_b	Diameter of cavity
V_s	EM wave velocity through host layer
V_b	EM wave velocity through cavity
T_c	Traveltime from ground surface to bottom of host layer through center of cavity
ε_b	Bulk dielectric permittivity of cavity material
ε_g	Dielectric permittivity of grains matrix
ε_w	Dielectric permittivity of water (= 80)
ε_a	Dielectric permittivity of air (= 1)

ε_s	Dielectric permittivity of host layer
ρ_b	Bulk density of cavity material
ρ_g	Density of grains matrix
ρ_w	Density of water (1000 kg/m^3)
ρ_a	Density of air (1 kg/m^3)
ρ_s	Density of the host layer
$\Delta\rho$	Density contrast
Δg_{max}	Maximum gravity change due to cavity
G	Universal gravitational constant (6.672×10^{-11} N m^2/kg^2)
$X_{1/2}$	Half width of the gravity anomaly curve at half of the maximum gravity effect due to cavity
z	Depth to center of cavity
R	Cavity radius
φ	Porosity of material inside cavity
S_w	Water saturation of material inside cavity

THESIS ABSTRACT

Name: Fathi Mohammed Saeed Abdullah

Title: Joint Inversion of Gravity and Ground Penetrating Radar Data to Characterize Subsurface Cavities

Degree: MASTER OF SCIENCE

Major Field: Geophysics

Date of Degree: May, 2014

Geophysics improves our understanding of subsurface geological features, such as cavities, that are important to characterize in many hydrogeological, environmental, and engineering studies. They are formed either naturally by the dissolution of limestones, dolomites, and evaporites or by human action, such as the construction of tunnels and tombs. Cavities can be filled with air, water, sediments, or a combination.

Gravity and ground penetrating radar (GPR) methods have already shown their ability to detect the location and size of subsurface cavities. The objective of this study is to present a new approach to determine the porosity and water saturation of cavity-filling materials using a quantitative joint inversion approach on GPR and gravity data sets.

The approach uses appropriate rock-physics models of GPR and gravity data above a subsurface cavity and inverts the porosity and water saturation in-

side the cavity by solving the two model equations simultaneously for these two variables. I test the proposed approach using synthetic GPR and gravity data sets corresponding to various cavity models. The results show that the method is accurate in retrieving the correct porosity and water saturation values within 2.5% error.

ملخص الرسالة

الاســـــــــم : فتحي محمد سعيد عبدالله

عنوان الرســـالة : توصيف التكهفات التحت سطحية بإستخدام النمذجة العكسية المشتركة من بيانات الجاذبية والرادار الأرضي المخترق.

الدرجـــة العلمية : ماجستير

التخـــصـــــص : جيوفيزياء

تـــاريخ التخرج : مايـــو 2014

ساهمت العلوم الجيوفيزيائية بشكل فعال في فهم الظواهر الجيولوجية التحت سطحية مثل ظاهرة التكهفات الشائعة التواجد في الصخور الجيرية، الدولوميت والمتبخرات. حيث تعتبر هذه الظاهرة مهمة جداً في الدراسات البيئية و الجيوهندسية والهيدروجيولوجية. وتتشكل هذه التكهفات إما طبيعياً نتيجة للإذابة التي تتعرض لها تلك الصخور الجيرية والمتبخرات أو بفعل النشاطات التي يقوم بها البشر على ظهر هذه الأرض كحفر الأنفاق والقبور. وقد تمتلئ هذه التكهفات بالمياة، بالرواسب أو ممتلئة بالهواء.

إن طرق الجاذبية الأرضية Gravity والرادار الأرضي المخترق GPR أظهرتا بشكل فعال كفائتيهما في تحديد أحجام و أماكن تواجد هذه التكهفات تحت السطح. ولكن الهدف من هذه الدراسة هو تقديم منهجية أو طريقة جديدة لإستخدام بيانات هاتين الطريقتين الجيوفيزيائيتين كنمذجة عكسية مشتركة لتحديد وحساب بعض المعاملات البتروفيزيائية للمواد الممتلئة بها هذه التكهفات مثل حساب قيمة المسامية porosity و التشبع بالمياة water saturation.

تبدأ هذه المنهجية من استخدام نموذج فيزيائي صخري Rock-Physics models مناسب في كلاً من الجاذبية والرادار الأرضي المخترق GPR لنفس منطقة التكهف التحت سطحي ومن ثم عمل نمذجة عكسية مشتركة

Joint Inversion لإستنباط قيمة المسامية Porosity والتشبع بالمياة Water Saturation للمواد داخل هذا التكهف من خلال الحل الرياضي لمعادلات تلك النماذج او الموديلات Models بشكل متزامن Simultaneously. ثم تم اختبار وفحص مصداقية وكفائة هذه الطريقة بإستخدام بيانات جاذبية ورادار مصطنعة Synthetic data لعدد من الحالات المفترضة لنوعية المواد المتواجدة داخل هذا التكهف مثلاً كأن يمتلئ بالهواء أو بالماء أو بالرمل الجاف أو الرمل المشبع بالمياة.

وبالأخير فإن النتائج التي تم الحصول عليها تبين أن هذه الطريقة ذات مصداقية دقيقة وذات كفائة جيدة في حساب القيم الصحيحة للمسامية والتشبع بالمياة للرواسب التي تمتلئ بها التكهفات التحت سطحية.

Chapter 1

INTRODUCTION

1.1 Overview

Geophysics improves our understanding of subsurface geological features. During the middle of the 20th century, GPR and gravity methods were rapidly developed to investigate subsurface problems (Reynolds, 1997). However, the last three decades have featured the most important achievements in application of both GPR and gravity methods in several fields, such as archaeology, engineering and environmental science. The use of GPR has increased in detecting and identifying many subsurface features, such as mineshafts, pipelines, ore lodes, cavities, groundwater, and buried rock valleys (Chamberlain et al., 2000).

Subsurface cavities are hazardous due to their susceptibility to ground surface subsidence, which can cause great losses to the population that occupies the land above them (Benson, 1995). Cavities are formed either naturally through the dissolution of limestones, dolomites, and evaporites or by human action, such as the construction of tunnels and tombs (Chalikakis et al., 2011). Cavities may be filled with air, water, sediments, or a combination.

There are many geophysical techniques that are appropriate for detecting and/or defining cavities features in the subsurface. For instance, microgravity (Butler, 1984; Bishop, 1997; Styles *et al.*, 2005 and Pánisová *et al.*, 2009), ground penetrating radar (Momayez *et al.*, 1996; Chamberlain *et al.*, 2000; Pipanet *et al.*, 2002), electrical resistivity tomography (Gambetta *et al.*, 2011; Putiska *et al.*, 2012 and Metwaly *et al.*, 2013), seismic refraction and reflection (Pernod *et al.*, 1989 and Fiore *et al.*, 2011) and transient electromagnetic methods (TEM) (Xue *et al.*, 2004). The strength of the GPR and gravity methods to detect subsurface cavities is mainly due to their ability and relative ease of detecting the contrast in physical properties between the surrounding soil or rock and the materials that fill these cavities.

The GPR and gravity methods are nondestructive geophysical techniques that measure differences in the physical properties of the subsurface materials, such as the dielectric permittivity for GPR and the density contrast for gravity. The success of the GPR and gravity methods depends on the different subsurface materials having different dielectric permittivities and bulk densities, which produce variations in the measured electromagnetic wave velocity (due to

variations in matrix composition and water content) and gravity field.

The joint inversion of geophysical data is becoming a more reliable approach to minimize uncertainty in the inversion of geophysical data between the observed data and the assumed model. The geophysical data, for example, GPR and microgravity, which are sensitive to the same physical quantity, can be simultaneously inverted by optimizing objective functions that include the same physical parameters, such as porosity and water saturation. the proposed methodology, in this study, is a joint inversion of GPR and gravity data to determine the water saturation and porosity of the cavity-filling material.

1.2 Literature Review

The literature records many studies describing qualitative investigations of cavities via utilizing several geophysical tools. Colley (1963) presented and discussed a few typical negative gravity anomalies related to shallow cavities in large caverns in Iraq. Butler (1984a) showed that the main components of subsurface cavity complex systems could be detected with microgravity measurements. He developed the initial physical geological models by computing the second and third derivatives of the gravity potential. In addition, Butler (1984b) used microgravimetric and gravity gradient techniques and concludes that these procedures are effective tools to the delineation and detection of shallow subsurface tunnels and cavities.

Chamberlain *et al.* (2000) presented promising results from using GPR for detecting cavities in limestone in an area of archaeologically important karst topography. While, Beres *et al.* (2001) combined GPR and microgravimetric methods as tools for detecting and characterizing shallow subsurface karstic features in terms of shape, size and depth. Al-Shuhail *et al.*, (2004) used GPR to delineate near-surface fractures within Dammam Dome and they concluded that GPR techniques can be used successfully to map near-surface open and filled fractures.

Ghose and Slob (2006) proposed a new idea in using GPR and seismic data quantitatively for estimating water saturation and porosity in subsoil using a shared earth model and they tested this approach through numerical simulations. Pánisová (2009) showed that local density variations caused by a near surface void resulted in negative anomalies detectable using microgravity techniques. Gembetta *et al.* (2011) suggested that using vertical gradient microgravity and electrical resistivity tomography, one can give high-resolution images of underground voids.

Fiore *et al.* (2011) reported that the shallow cavities in tuff layer characterized by a high acoustic impedance contrast can be easily detected with a high resolution P-wave seismic reflection technique. Hajian *et al.* (2012) applied a new approach for modeling subsurface cavities characterized by typical geometries such as sphere, vertical and horizontal cylinder by using a linear neuro-fuzzy microgravity technique. Metwaly and AlFouzan (2013) described a 2D electrical resistivity survey in a newly urbanized area in Alhassa of Saudi

Arabia and they found that the method is useful to delineate different cavities.

1.3 Motivation

The presence of cavities features in the subsurface rock and their potential collapse pose an acute geohazard and constitute a risk to developed land. The delineation of subsurface cavities and the determination of porosity and water saturation parameters of cavity filling materials are important in many geotechnical applications. Drilling is a common method of site investigation in an attempt to detect and characterize physical parameters of subsurface cavities such as porosity and water saturation but it is expensive. In order to overcome this issue, non-invasive and cost-effective geophysical methods can be used for cavity detection. Due to the importance of estimating porosity and water saturation to civil engineers in designing better structures, a joint inversion approach of GPR and gravity data is proposed for calculating these two parameters.

1.4 Problem Statement

To date there have not been attempts at GPR and gravity petrophysical joint inversion cited to estimate porosity and water saturation of cavity filling materials. However, most previous GPR and gravity studies have been applied as integration on subsurface cavity detection using qualitative approach. In

this thesis, the objective is to develop a new petrophysical joint inversion using GPR and gravity data sets. It is intended to be applied to estimate important petrophysical parameters of the material inside cavities which are porosity and water saturation. Therefore, the aim of this work is to develop, test and apply a GPR and gravity joint inversion approach. Joint inversions gather data sets from complementary GPR and gravity techniques measured in the same area over the same subsurface cavities. Furthermore, this data is simultaneously inverted with respect to porosity and water saturation.

1.5 Thesis Objectives

The aim of this work is to provide an efficient approach that combines gravity and GPR data sets to determine porosity and water saturation of subsurface cavities filling materials. The developed methodology is considered a quantitative approach by using a joint inversion technique. Then, this new approach is tested using synthetic GPR and gravity data sets.

1.6 Thesis Outline

A general outline of the thesis chapters is organized as follows. Chapter 1 presents a general introduction and literature review of cavity investigations using geophysical tools. In chapter 2, the general principles of gravity and

GPR methods are described. Furthermore, a new procedure for calculating porosity and water saturation of cavity-filling materials using a joint inversion approach is derived. This derivation consists of two steps: the equations for the GPR and gravity methods are formulated for selected models and the resulting equations are solved simultaneously by close form solution to obtain the equation of porosity and water saturation. The developed methodology is tested using synthetic gravity and GPR data sets for five models. The generation of synthetic data for all models is presented in chapter 3. This is followed in chapter 4 by testing this new approach to estimate the porosity and water saturation of these synthetic data and discussion of all the results. Furthermore, a sensitivity analysis is presented at the end of chapter 4. Finally, conclusions and some recommendations are provided in chapter 5.

Chapter 2

METHODS AND PROCEDURES

2.1 Overview

The detection of cavities is possible using geophysical methods because the presence of a cavity changes the physical properties of the subsurface rocks and causes a physical contrast between the cavity materials and the surrounding environment. This chapter provides the general concepts and basic principles of gravity and GPR methods. In addition, the joint inversion methodology to achieving the thesis objectives are addressed.

2.2 Gravity Method

The gravity method measures the lateral variation in the vertical component of the gravitational field at the Earths surface. This variation is due to the subsurface density distribution. Moreover, this technique is appropriate to the investigation of subsurface geological features, such as tracing of geological boundaries and mapping of sedimentary basins. Cavities can be filled with air, water, sediments or a combination. Therefore, cavities usually have a lower density than the surrounding rocks. and produces a very small negative gravity anomaly.

Over the last ten years, microgravity surveying has developed considerably in several aspects. These improvements include the development of high-resolution instruments such as the Burris Gravity Meter (Mochales *et al.*, 2008) with a precision of $1\mu Gal$ ($1\mu Gal = 10^{-6} cm/s^2$), improved designs for field acquisitions, high-quality data correction methods and improved analysis procedures. As a result, it is possible to delineate and interpret anomalies as small as 10 μGal and this method also provides useful information about the depth, shape and geometry of cavities . In addition, there are laser levels with precisions greater than 1 mm such as the LEICA Sprinter, which the topographic elevation can be accurately measured (Mochales *et al.*, 2008).

In general, Newtons Law of gravitation is the basic law that addresses gravity measurements:

$$F_g = G\frac{M_1 M_2}{R^2} \tag{2.1}$$

where Fg is the gravitational force due to the two masses M1 and M2, G is the universal gravitational constant (6.672 x $10^{-11} N.m^2/kg^2$), M1 and M2 are the two masses and R is the distance between them.

From equation 2.1, the gravitational acceleration (g) due to a body of mass M is:

$$g = \frac{GM}{R^2} \tag{2.2}$$

Gravitational acceleration, g, is measured in Gal (after Galileo), where 1 Gal = 0.01 m/s^2. However, most targets of interest usually produce much smaller anomalies, especially in engineering and environmental studies. Consequently, these studies require surveys with μGal resolution ($1\mu Gal = 0.001 mGals$). In this case, the term "Microgravity survey" is used instead of "Gravity Survey", which is generally used for regional gravity surveys. For more information on the basics of the gravity method, see Nettleton (1976) and Telford *et al.* (1990).

Cavities can be modeled as spherical bodies. The basic equation for the effect on gravity of a spherical body is given in equation 2.3 (Nettleton, 1940). These parameters are depicted in Figure 2.1, where (R) is the radius of the sphere, (z) is the depth to the sphere's center, ($\Delta\rho$) is the density contrast

between spherical body and surrounding materials, (ρ_b) is the density of the body and (ρ_s) is the density of the surrounding rock:

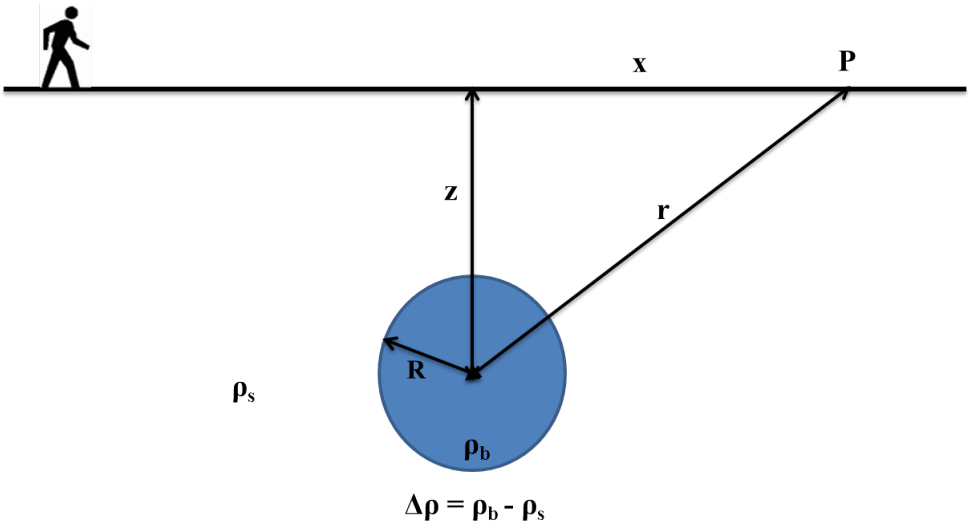

Figure 2.1: Schematic diagram showing a spherical body and the parameters that affects its gravity anomaly.

$$g_z = \frac{AGz}{(x^2 + z^2)^{3/2}} \tag{2.3}$$

where $A = \frac{4}{3}\pi R^3 \Delta\rho$

The maximum gravity anomaly lies directly over the center of cavity where $x = 0$ and the equation 2.3 reduces to the following form:

$$g_{max} = \frac{AG}{z^2} \tag{2.4}$$

In the rock-physics model, the porosity-density relationship describes the bulk density of sedimentary rocks. Moreover, the phases used to describe sedimentary rocks are the rock grains and the pore voids, which may be filled with water and/or air(Figure 2.2).

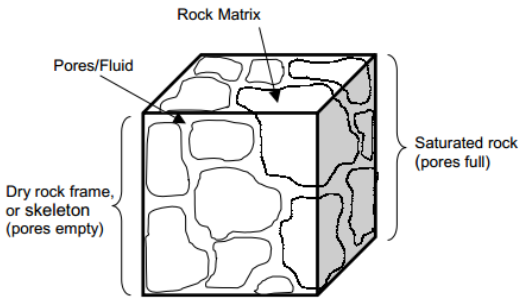

Figure 2.2: Schematic representation of a partially-saturated sedimentary rock with grains, air and water (Russell *et al.*, 2003).

.

The bulk density can be described as the sum of any number of components, weighted by their fractional volumes. One such variation is to allow fractional degrees of saturation, as shown in Figure 2.2, and the porosity-density relationship (volume average equation) is given as

$$\rho_b = \rho_g(1-\phi) + \rho_f\phi, \tag{2.5}$$

where

$$\rho_f = S_w\rho_w + (1-S_w)\rho_a, \tag{2.6}$$

giving:

$$\rho_b = \rho_g(1-\phi) + S_w\rho_w\phi + \phi(1-S_w)\rho_a \tag{2.7}$$

2.3 Ground Penetrating Radar

Ground Penetrating Radar (GPR) is a non-destructive method that generates EM pulses to record and locate the depth of buried objects or subsurface features that cannot be seen visually (Do, 2003). In the last three decades, the GPR technique has become an effective method for detecting shallow buried targets (Luo *et al.*, 2005).

GPR method is based upon the propagation and reflection characteristics of an EM wave through a material. An EM wave is reflected off the targets due to a change in the EM properties of subsurface objects, such as the dielectric permittivity (ϵ), the magnetic permeability (μ) and electrical conductivity (σ) (Daniels, 2004; Scheele, 2011).

An interface is an abrupt change in the electrical or magnetic material properties. Reflection and refraction result when a propagating EM wave encounters an interface that extends over large distances, compared to the wavelength and the reflected part of the wave is recorded in terms of its two-way travel time and amplitude for analysis and interpretation stages according to the objectives (Dojack, 2012). The velocity of electromagnetic waves in subsurface materials is given as:

$$v = \frac{c}{\sqrt{\epsilon_b \mu_r \frac{1+\sqrt{1+(\frac{\sigma}{\omega\epsilon_b})^2}}{2}}} \tag{2.8}$$

where $\omega = 2\pi f$ is the angular frequency, c is the EM wave velocity in vacuum (0.3 m/ns), ϵ_b denotes the dimensionless bulk relative dielectric permittivity, μ_r is the dimensionless relative magnetic permeability, σ is the electrical conductivity of the medium in units of (Siemens/m), and $\sigma/\omega\epsilon_b$ is the loss factor. However, in materials with no conductivity ($\sigma = 0$) and no magnetic properties ($\mu_r = 1$), equation 2.8 becomes (Davis and Annan, 1989):

$$v = \frac{c}{\sqrt{\epsilon_b}} \tag{2.9}$$

Resolution is defined as the ability to distinguish two closely spaced reflections. It is mainly controlled by the EM wavelength. However, it can also be affected by other factors such as polarization of the EM energy, the reflection coefficient, geometrical aspects of the target, and noise. In addition, the rate of spatial change in properties between the target and the host medium plays an important role in determining resolution. Generally, resolution increases as the change becomes sharper and decreases as the change becomes gradational (Olhoeft, 2000). Furthermore, there is a trade-off between resolution and penetration depth. Resolution increases with frequency, while penetration depth decreases with frequency (Conyers, 2004; Grealy, 2006). For more information on the principles of GPR, see Davis and Annan (1989).

The electrical properties of porous rocks are sensitive to the volume fractions of the solid and fluid phases. Additionally, the most important factors

in determining the dielectric constant of near-surface materials are the porosity and water saturation. The complex refractive index model (CRIM) is a widely used formula for expressing the bulk dielectric permittivity of a material as a function of its porosity and water saturation. The formula is based on a volumetric averaging of the dielectric constants of the constituents of composite materials (Tsui and Matthews, 1997):

$$\sqrt{\epsilon_b} = \phi(1 - S_w)\sqrt{\epsilon_a} + (1 - \phi)\sqrt{\epsilon_g} + \phi S_w\sqrt{\epsilon_w} \tag{2.10}$$

2.4 Joint Inversion Methodology

The new joint inversion approach combines gravity and GPR data in a petrophysical approach using appropriate rock-physics models of the porosity-density relationship and the CRIM.

2.4.1 The basic idea

A gravity and GPR joint inversion requires a link between the two techniques. Therefore, porosity and water saturation were established as the crucial link between dielectric permittivity and density through the porosity-density relationship (Eq. 2.7) and CRIM (Eq. 2.10). Thus, these petrophysical properties provide a useful link in the joint inversion approach to determine the porosity

and water saturation from GPR and gravity data sets.

The joint inversion technique, in which multiple geophysical data sets are analyzed and inverted simultaneously, represents an expanding field in geophysics. As a result, uncertainty in interpretations will be reduced. In this thesis, a new joint inversion approach for gravity and GPR data sets has been developed.

The gravity and GPR methods were selected for this thesis because they are popular techniques in cavity investigations and in near-surface geophysics applications. In addition, the theory of these techniques is relatively simple, which helps us to develop a new joint inversion approach to determine porosity and water saturation from other geophysical methods.

2.4.2 Methodology

The main aim of this thesis is to develop and test a joint inversion of gravity and GPR data sets to determine the porosity and water saturation of cavity-filling materials. In this case, the data sets from two complementary geophysical methods, measured over the same subsurface cavity, are simultaneously inverted to calculate the values of porosity and water saturation of the materials within the cavity.

To achieve the objectives presented in chapter 1, the following approach is adopted. In the initial steps of this new approach, the basic model (Fig. 2.3)

features a cavity that is spherical in shape and filled with sediments, air, water or a combination of two or more phases.

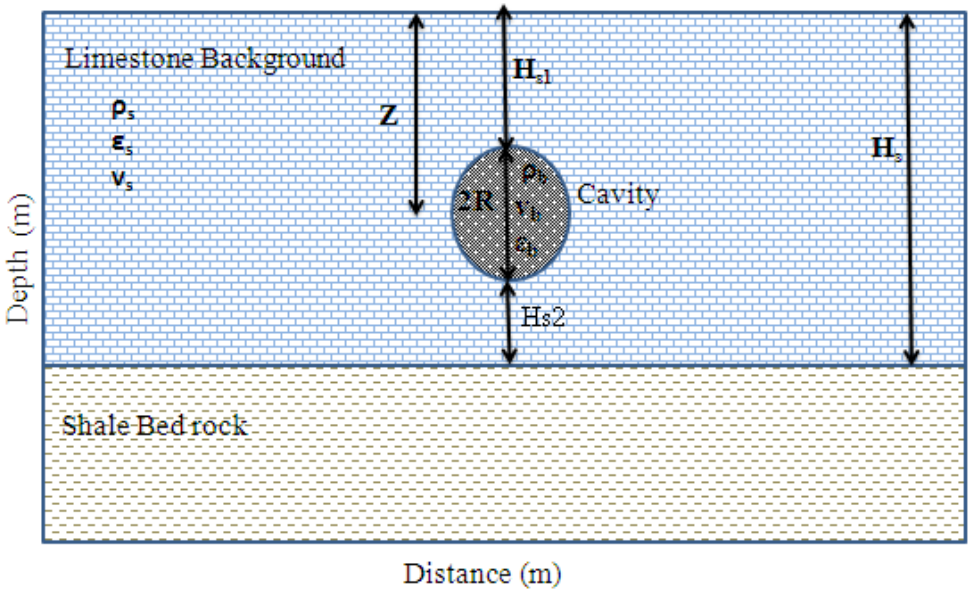

Figure 2.3: Illustration of parameters used in GPR equations.

Now, according to basic model (Fig. 2.3), one can obtain the relationships that are important to formulate the general equations, which will be solved later with respect to porosity and water saturation.

$$H_{s1} = z - R \tag{2.11}$$

$$H_{s2} = H_s - (z + R) \tag{2.12}$$

$$H_b = 2R \tag{2.13}$$

$$R = z - H_{s1} \tag{2.14}$$

$$T_0 = \frac{2H_s}{V_s} \tag{2.15}$$

$$H_s = \frac{T_o V_s}{2} \tag{2.16}$$

$$V_b = \frac{0.3}{\sqrt{\epsilon_b}} \tag{2.17}$$

$$T_c = T_{s1} + T_b + T_{s2} \tag{2.18}$$

Then

$$T_c = \frac{2H_{s1}}{V_s} + \frac{2H_b}{V_b} + \frac{2H_{s2}}{V_s} \tag{2.19}$$

In this approach, the GPR travel times are used directly, without the need to create a velocity tomogram. This is one of the benefits of this approach.

Subsequently, it is easy to invert equation 2.19 with respect to V_b and obtain the following equation:

$$V_b = \frac{4RV_s}{V_s T_c - 2H_s + 4R} \tag{2.20}$$

Substituting equation 2.20 into equation 2.9, I obtain the following general equation of dielectric permittivity of cavity-filling materials, where $x_{1/2}$ is the half-width of the anomaly curve at half of the maximum gravity anomaly value (Fig. 2.4):

$$\sqrt{\epsilon_b} = \frac{0.3[V_s T_c - 2H_s + 4(1.305x_{\frac{1}{2}} - H_{s1})]}{4V_s(1.305x_{\frac{1}{2}} - H_{s1})} \tag{2.21}$$

Finally, by substituting equation 2.21 into equation 2.10, the general equation deduced from the GPR data for a spherical cavity can be written as:

$$\frac{0.3[V_s T_c - 2H_s + 4(1.305x_{\frac{1}{2}} - H_{s1})]}{4V_s(1.305x_{\frac{1}{2}} - H_{s1})} = \phi(1 - S_w)\sqrt{\epsilon_a} + (1 - \phi)\sqrt{\epsilon_g} + \phi S_w\sqrt{\epsilon_w} \tag{2.22}$$

In the same manner, the effects of cavity-filling materials on gravity are expressed in a general equation that can be derived from a gravity profile, as illustrated in Figure 2.4.

Now, the relationships below can be written based on a spherical cavity model (Fig. 2.4). The bulk density of the cavity materials is expressed as:

$$\rho_b = \rho_s + \Delta\rho \tag{2.23}$$

As mentioned earlier, the maximum gravity anomaly lies directly over the center of the spherical cavity, where x = 0, (equation 2.4).

To identify the bulk density of the cavity material, equation 2.4 is rewritten with respect to $\Delta\rho$ as follows:

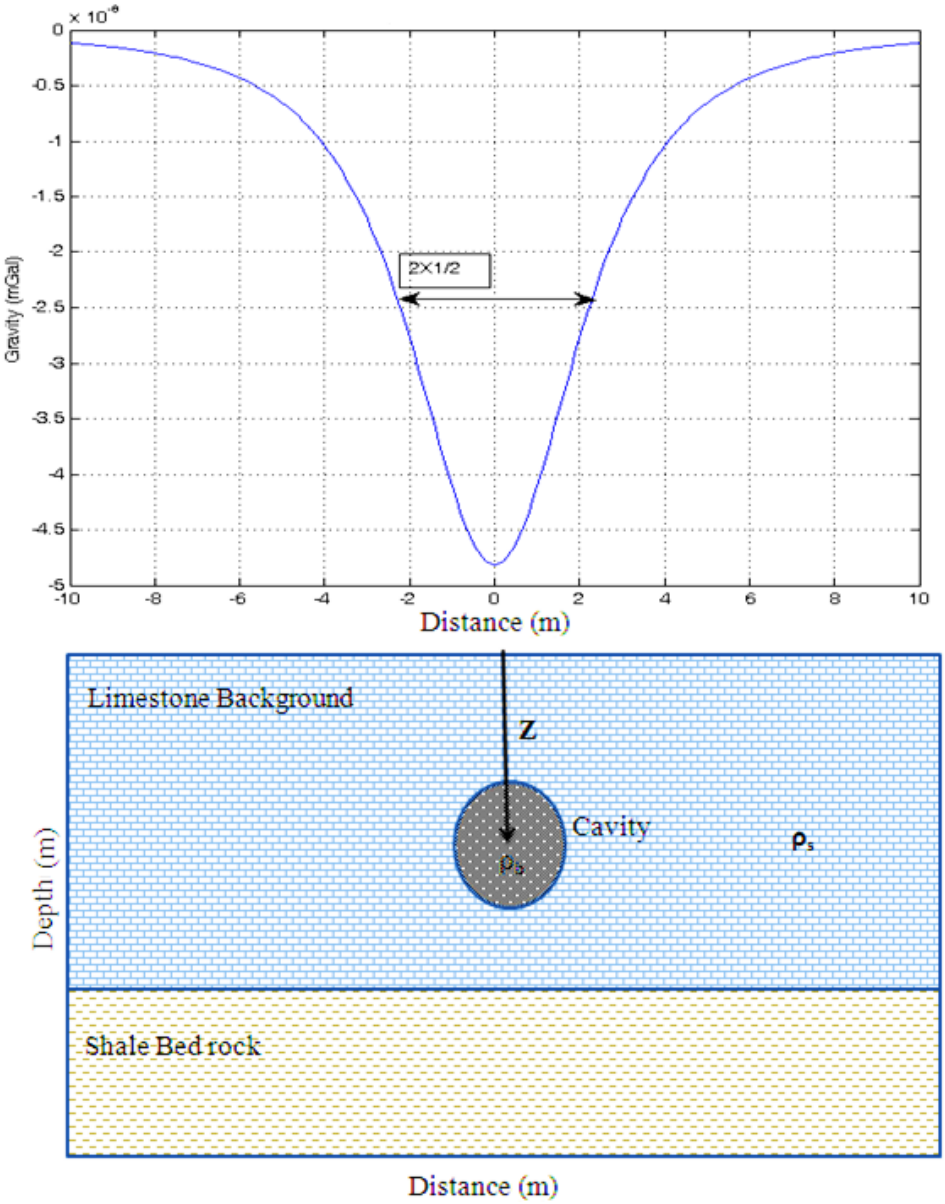

Figure 2.4: (upper) gravity anomaly curve over cavity, (lower) spherical cavity model within a limestone bed.

$$\Delta\rho = \frac{3Z^2 g_{max}}{4\pi G R^3} \tag{2.24}$$

Substituting equation 2.24 into equation 2.23, the following general equation of the bulk density of cavity materials is obtained:

$$\rho_b = \frac{3Z^2 g_{max}}{4\pi G R^3} + \rho_s \tag{2.25}$$

From the rule of the half-width method (Nettleton, 1942), the depth to the center of the spherical cavity can be estimated by using this empirical formula: $z = 1.305$ x $x_{1/2}$, where $x_{1/2}$ is the width of the anomaly curve at half of the maximum gravity anomaly (Fig. 2.4). Moreover, the radius of the cavity can be estimate from GPR data, discussed previously as $R = z - H_{s1}$. Hence, equation 2.25 becomes the following:

$$\rho_b = \frac{3(1.305 x_{\frac{1}{2}})^2 g_{max}}{4\pi G(1.305 x_{\frac{1}{2}} - H_{s1})^3} + \rho_s \tag{2.26}$$

Finally, by substituting the value of ρ_b from equation 2.26 into the density-porosity relationship (Eq. 2.7), the general equation deduced from the gravity data can be written as:

$$\frac{1.27(x_{\frac{1}{2}})^2 g_{max}}{\pi G(1.305 x_{\frac{1}{2}} - H_{s1})^3} + \rho_s = \rho_g(1-\phi) + S_w\rho_w\phi + \phi(1-S_w)\rho_a \tag{2.27}$$

According to assumptions at the beginning of the methodology section and the information deduced from both of the gravity anomaly curve and the

radargram data, all the parameters in equations 2.22 and 2.27 are known except S_w and ϕ.

As an illustration, the depth to the center of cavity z and $x_{1/2}$ can be obtained from the gravity curve, while the H, H_{s1} and H_{s2} can be calculated from travel time picking on the radargram. Moreover, there are many constants, such ρ_g, ρ_w, ρ_a, ϵ_g, ϵ_w, ϵ_a and G, that are tabulated in most geophysical references (e.g., Telford *et al.*, 1997)

Because all other parameters in equations 2.22 and 2.27 are known, these two equations can be solved simultaneously for ϕ and S_w, to give the following solutions:

$$\phi = \frac{CM - AD}{CN - BD} \tag{2.28}$$

$$S_w = \frac{-BM + AN}{CM - AD} \tag{2.29}$$

where

$A = \frac{1.27(x_{\frac{1}{2}})^2 g_{max}}{\pi G(1.305 x_{\frac{1}{2}} - H_{s1})^3} + \rho_s - \rho_g$,

$B = \rho_a - \rho_g$,

$$C = \rho_w - \rho_a \ ,$$

$$D = \sqrt{\epsilon_w} - \sqrt{\epsilon_a} \ ,$$

$$M = \frac{0.3(v_s T_c - 2H_s + 4(1.305x_{\frac{1}{2}} - H_{s1}))}{4v_s(1.305x_{\frac{1}{2}} - H_{s1})} - \sqrt{\epsilon_g} \text{ and}$$

$$N = \sqrt{\epsilon_a} - \sqrt{\epsilon_g}$$

Next, the new joint inversion methodology approach is applied to estimate the porosity and water saturation of cavity materials using synthetic gravity and GPR data sets.

Chapter 3

SYNTHETIC GPR AND GRAVITY DATA SETS

3.1 Overview

This chapter aims to generate synthetic GPR and gravity data for a cavity model with the following five types of cavity-filling materials:

- Model 1: Cavity filled with pure air.
- Model 2: Cavity filled with pure water.
- Model 3: Cavity filled with dry sand.
- Model 4: Cavity filled with partially saturated sand.

- Model 5: Cavity filled with fully saturated sand.

These synthetic data are used to validate this new approach for estimating the porosity and water saturation of cavity materials.

The procedure followed to generate GPR and gravity synthetic data through forward modelling is illustrated in Figure 3.1. For a given subsurface model that reflects the distribution of target parameters (porosity and water saturation), this model can be converted to subsurface dielectric model using a suitable rock physics model (CRIM). Then, the GPR synthetic data is produced using a forward modeling split-step algorithm. On the other hand, in the case of gravity, the subsurface properties distribution is converted to subsurface densities model through porosity-density relationship. Then, the predicted gravity anomaly curve is calculated through analytical expression of sphere and horizontal slab as depicted in Figure 3.1.

3.2 GPR Synthetic Data

In this section, GPR simulations have been computed using a two-dimensional split-step algorithm (Bitri and Grandjean, 1998). This method is a full-waveform method that requires the solution of Maxwell's equations in the frequency domain, and it is implemented via MATGPR (Tzanis, 2010), which is an EM wave simulator for GPR modeling based on the split-step numerical

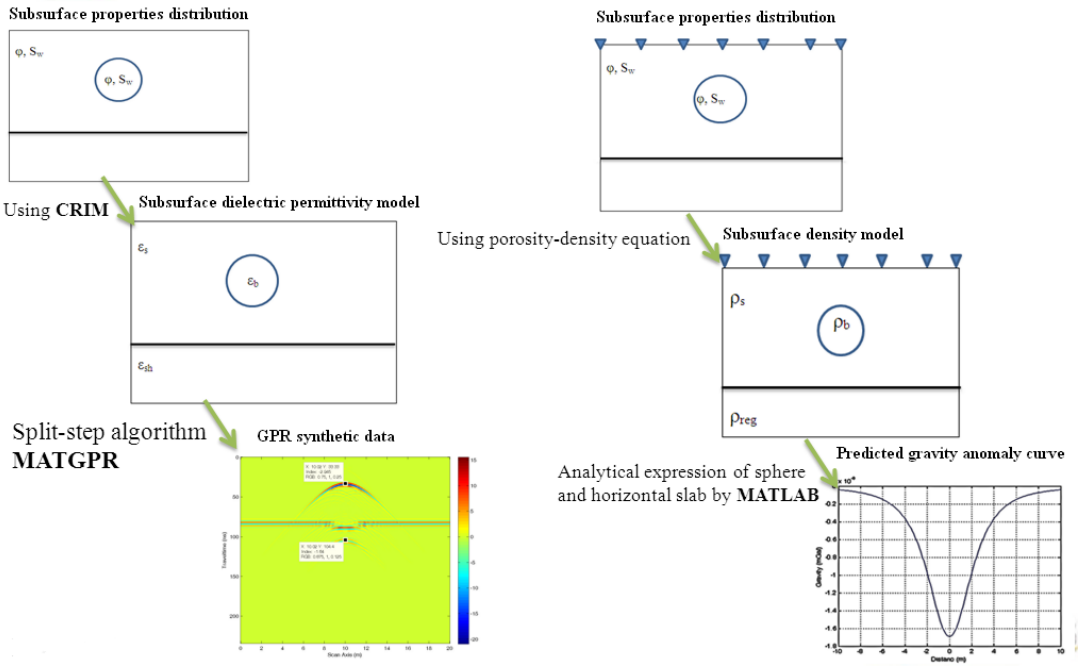

Figure 3.1: Schematic illustration of the forward modeling procedure to generate GPR and gravity data.

method. The basic model shown in Figure 3.2 has horizontal and vertical dimensions of 20 m and 10 m, respectively, and a grid spacing of 1 m in both directions. Additionally, there is a horizontal interface at 5 m, which separates the upper limestone layer and the lower shale bedrock. There is also a spherical cavity in the upper layer with a radius of 1 m, and its center is located at a depth of 3 m and a horizontal distance of 10 m. For each model, the sediment grains dielectric permittivity was assigned a value of $\epsilon_g = 4.5$ (assuming pure quartz sand grains), the water permittivity was $\epsilon_w = 80$ and $\epsilon_a = 1$ for air dielectric permittivity, the center frequency of the EM wave used in all GPR simulations is 250 MHz.

Models	Input parameters				
	$\varepsilon_g = 4.5$, $\varepsilon_w = 80$, $\varepsilon_a = 1$, $f = 250MHz$ $\rho_g = 2650(kg/m^3)$, $\rho_w = 1000(kg/m^3)$, $\rho_a = 1(kg/m^3)$				
	$\rho_b(kg/m^3)$	V(m/ns)	ϕ	S_w	ε_b
Cavity filled with pure air	1	0.2998	1	0	1
Cavity filled with pure water	1000	0.033518	1	1	80
Cavity filled with dry sand	1855.3	0.168	0.3	0	3.18596
Cavity filled with partially saturated sand	2005.15	0.1007	0.3	0.5	8.8599
Cavity filled with fully saturated sand	2155	0.071924	0.3	1	17.374
Limestone background	2550	0.12			6.25
Shale bed rock	2420	0.09			11.111

Table 3.1: Synthetic models of cavity materials and background parameters used in the generation of GPR and gravity data. Density values are from Telford *et al.* (1990) and dielectric values are from Annan *et al.* (1992).

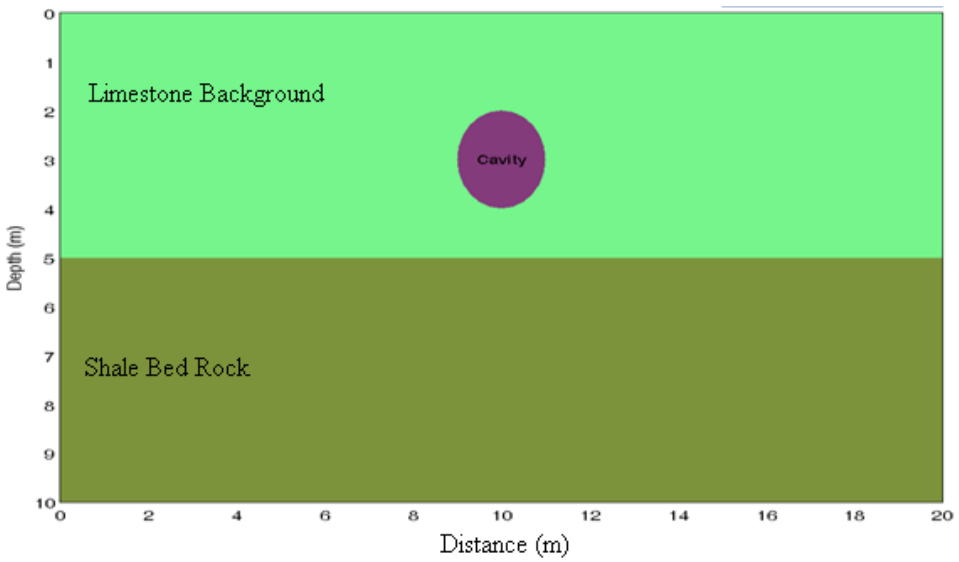

Figure 3.2: Illustration of basic model elements used in the generation of synthetic GPR and gravity data.

3.2.1 Model 1: Cavity filled with pure air

In this model, according to the CRIM, the dielectric permittivity of the cavity material is $\epsilon_b = 1$ and it has a high resistivity, producing an EM wave velocity through the cavity materials of 0.2998 m/ns. The limestone background has a dielectric permittivity of 6.25.

The synthetic radargram of this model is shown in Figure 3.3. The two synthetic layers and the positions of the top and bottom of the cavity are clearly shown. However, the variation between the different dielectric permittivities of each layer changes the two-way travel times, and it is controlled by the EM wave velocity through the various materials. In general, there is a horizontal event at 83.34 ns, which represents the horizontal interface between the limestone and shale layer at 5 m depth. In addition, there are two hyperbolas, which represent the top and bottom of the cavity. The most important event is the travel time to the interface directly beneath the cavity, which appears as a hyperbola at 63.56 ns. Figure 3.4 shows an extracted trace (No. 10) from Figure 3.3 that passes through the cavity and clearly shows the events described above.

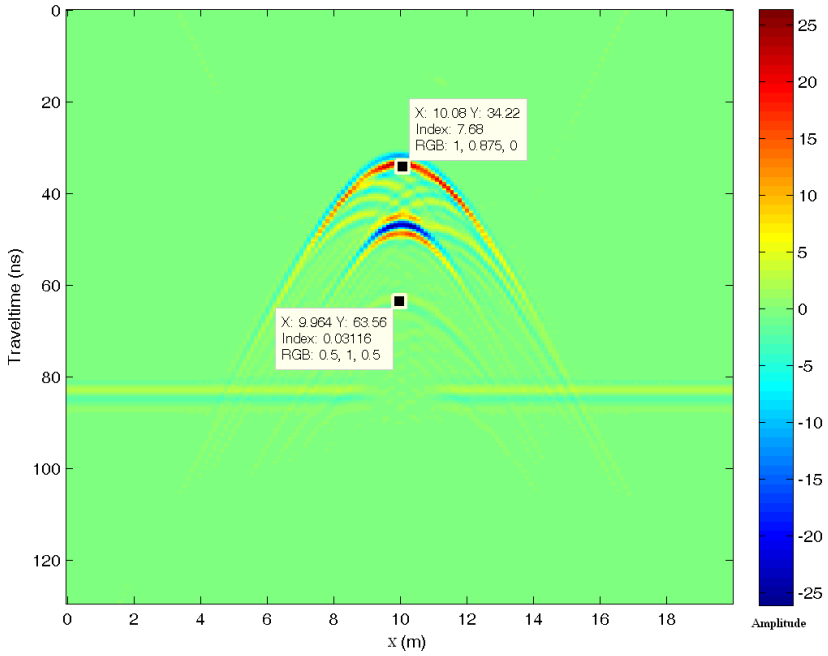

Figure 3.3: Synthetic radargram obtained from 250 MHz antenna for cavity filled with pure air.

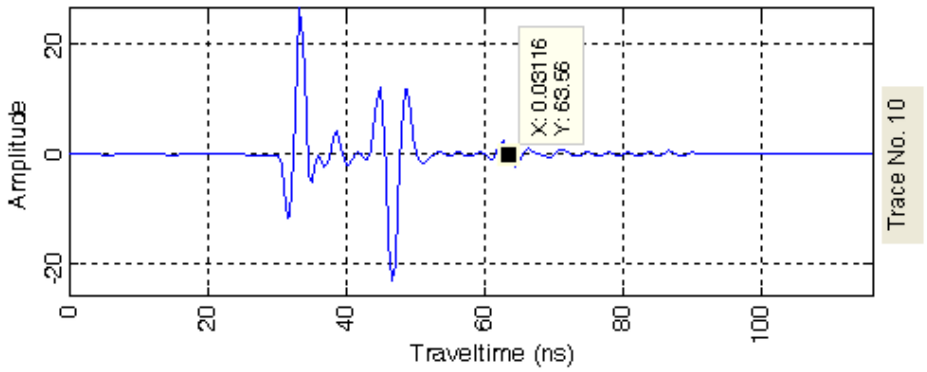

Figure 3.4: Trace extracted from synthetic GPR data shown in figure 3.3 at $x = 10$ through cavity.

3.2.2 Model 2: Cavity filled with pure water

In this model, the dielectric permittivity $\epsilon_b = 80$, and the EM wave velocity through the cavity materials is equal to 0.033518 m/ns.

In Figure 3.5, the synthetic radargram of this model is shown. The position of the top and the bottom of the cave in this figure is correctly detected. The travel time at the interface directly beneath the cavity is 170.7 ns. In this case, the reflection is weak due to the presence of water in the cavity, which attenuates the EM waves and decreases the velocity of the EM waves.

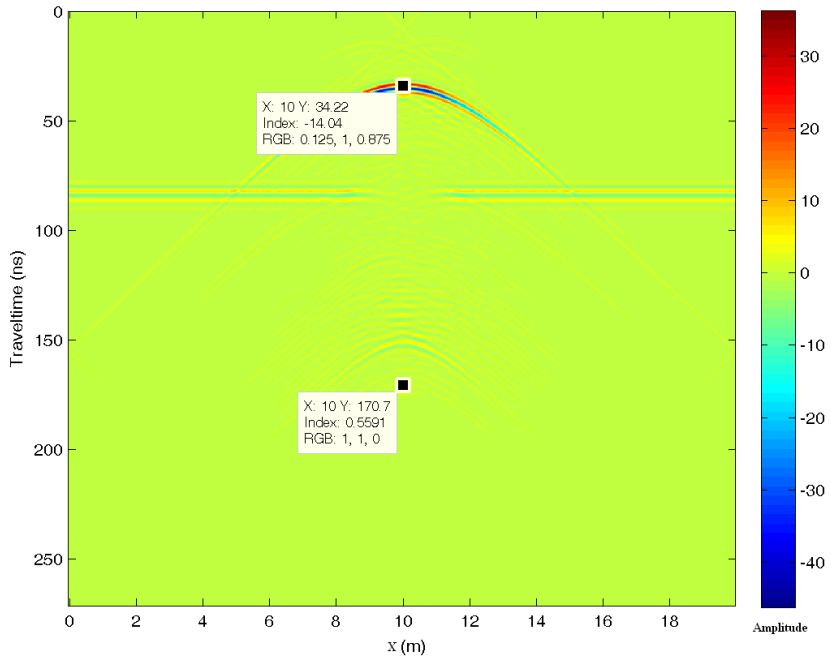

Figure 3.5: Synthetic radargram obtained from 250 MHz antenna for cavity filled with pure water.

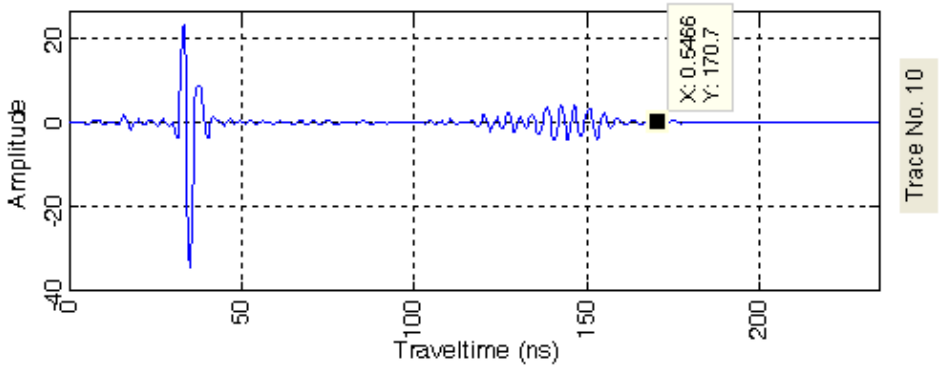

Figure 3.6: Trace extracted from synthetic GPR data shown in figure 3.5 at $x = 10$ through cavity.

3.2.3 Model 3: Cavity filled with dry sand

In this model, the cavity is filled with dry sand, and I assume the porosity is equal to 0.3 and the water saturation is equal to zero. The cavity has a dielectric permittivity of $\epsilon_b = 3.18596$, according to CRIM, and the EM wave velocity through the cavity materials is equal to 0.168 m/ns.

The synthetic radargram of this model is demonstrated in Figure 3.7. This figure shows that there are three important hyperbolic events, two of them represent the top and bottom of the cavity and the third is reflected from interface directly beneath the cavity at 74.22 ns.

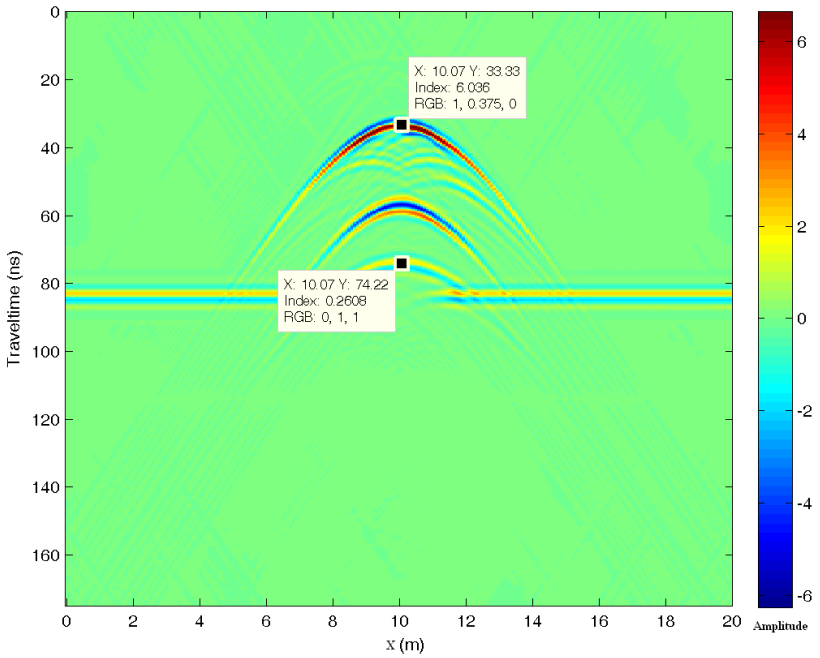

Figure 3.7: Synthetic radargram obtained from 250 MHz antenna for cavity filled with dry sand.

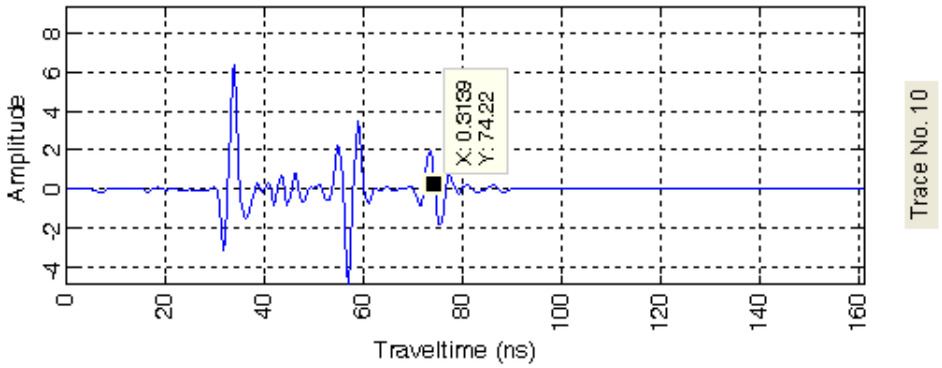

Figure 3.8: Trace extracted from synthetic GPR data shown in figure 3.7 at $x = 10$ through cavity.

3.2.4 Model 4: Cavity filled with partially saturated sand

In this model, the cavity is filled with partially saturated sand, which has a dielectric permittivity of $\epsilon_b = 8.8599$ because the assumed porosity and water saturation were 0.3 and 0.5, respectively. The EM wave velocity through the cavity materials is equal to 0.1007 m/ns.

The synthetic radargram of this model is displayed in Figure 3.9. The radargram shows that all synthetic interfaces appear clearly, including the cavity edges and the interface. The total travel time from the surface to the interface directly beneath the cavity is 89.33 ns.

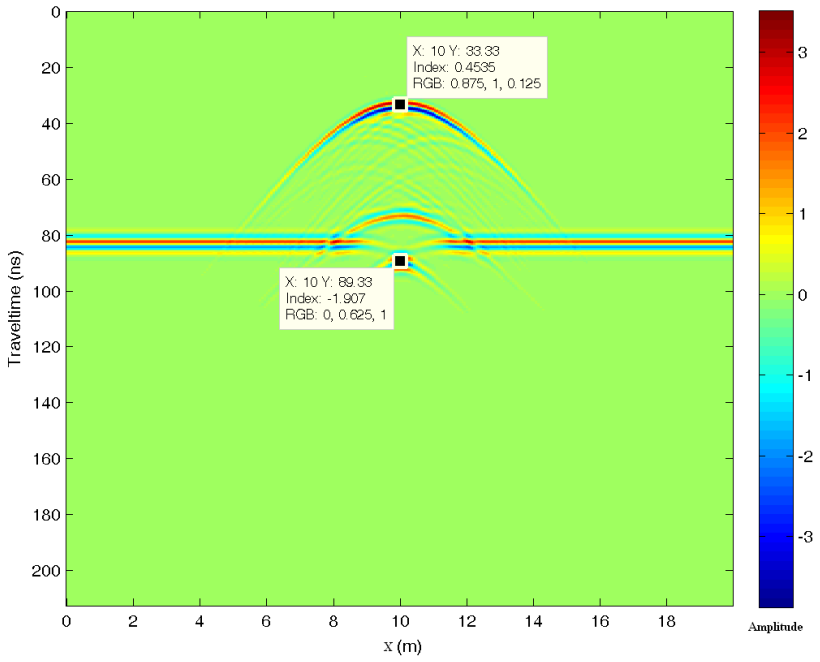

Figure 3.9: Synthetic radargram obtained from 250 MHz antenna for cavity filled with partially saturated sand.

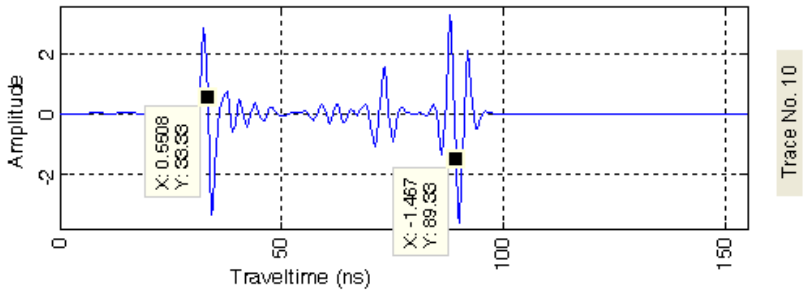

Figure 3.10: Trace extracted from synthetic GPR data shown in figure 3.9 at $x = 10$ through cavity.

3.2.5 Model 5: Cavity filled with fully saturated sand

In this model, the cavity is filled with fully saturated sand. In this case, the porosity is equal to 0.3, and the water saturation is 1.0. Therefore, it has a dielectric permittivity of $\epsilon_b = 17.374$, and the EM wave velocity through the cavity materials is equal to 0.071924 m/ns.

The synthetic radargram of this model is shown in Figure 3.11. The reflections are strong and show the top and bottom boundaries of the cavity, as well as the reflection event from the interface directly beneath cavity at 104.4 ns.

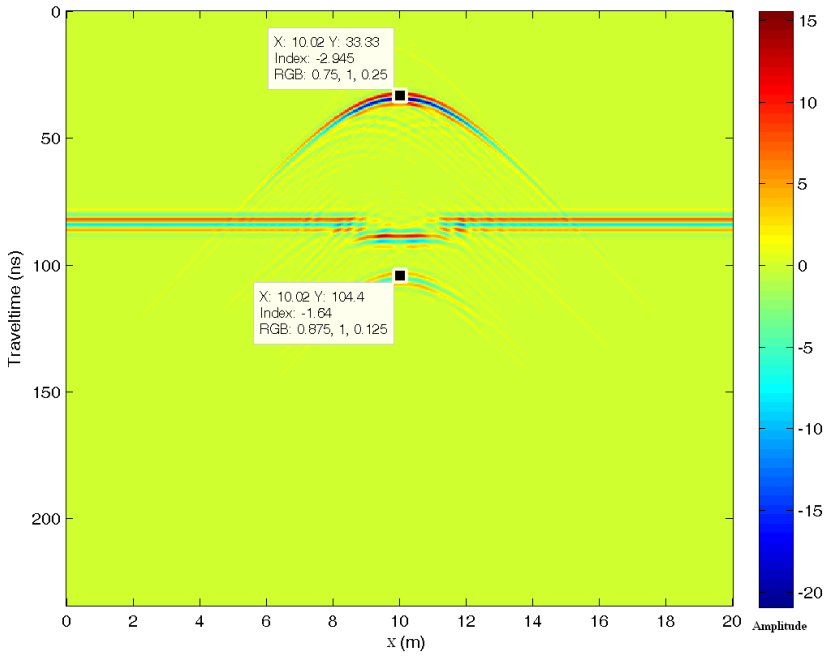

Figure 3.11: Synthetic radargram obtained from 250 MHz antenna for cavity filled with fully saturated sand.

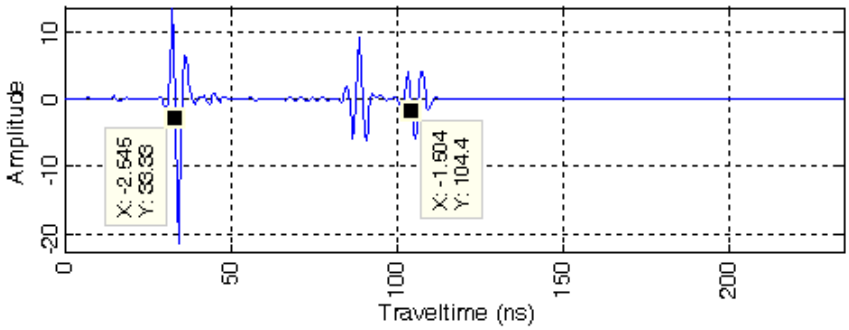

Figure 3.12: Trace extracted from synthetic GPR data shown in figure 3.11 at $x = 10$ through cavity.

3.3 Gravity Synthetic Data

The gravity synthetic data were generated for the five models (see Figs. 3.13 to 3.17) via a combination of the analytical expressions for a 2D horizontal slab, which represents a limestone background, and a spherical anomalous body, which represents the target cavity body. However, the Matlab function has been written to calculate the Bouguer gravity anomaly for those models. In this section, the basic model shown in Figure 3.2 has horizontal and vertical dimensions of 20 m and 10 m, respectively. There is a horizontal interface at 5 m, which separates the upper limestone layer and the lower shale bedrock. In addition, there is a spherical cavity in the middle of the upper layer with a radius of 1 m, and its center is located at 3 m depth. For each model, the matrix density was assigned a value of $\rho_g = 2650\ kg/m^3$, the water density was $\rho_w = 1000\ kg/m^3$ and $\rho_a = 1\ kg/m^3$ for the air density. The data generated from these models has already been corrected for Bouguer effects.

3.3.1 Model 1: Cavity filled with pure air

The gravitational effect of the anomaly in this model can be computed by considering the sum of two simple shapes, a horizontal sheet with a density of 2550 kg/m^3 and a thickness of 5 m, which represents the limestone background, and a spherical body with a density of 1 kg/m^3 and a radius of 1 m.

The residual Bouguer anomaly curve of this model is depicted in Figure 3.13. It shows that the maximum gravity anomaly directly over the center of the cavity is $g_{max} = -0.0000792 \mu Gal$.

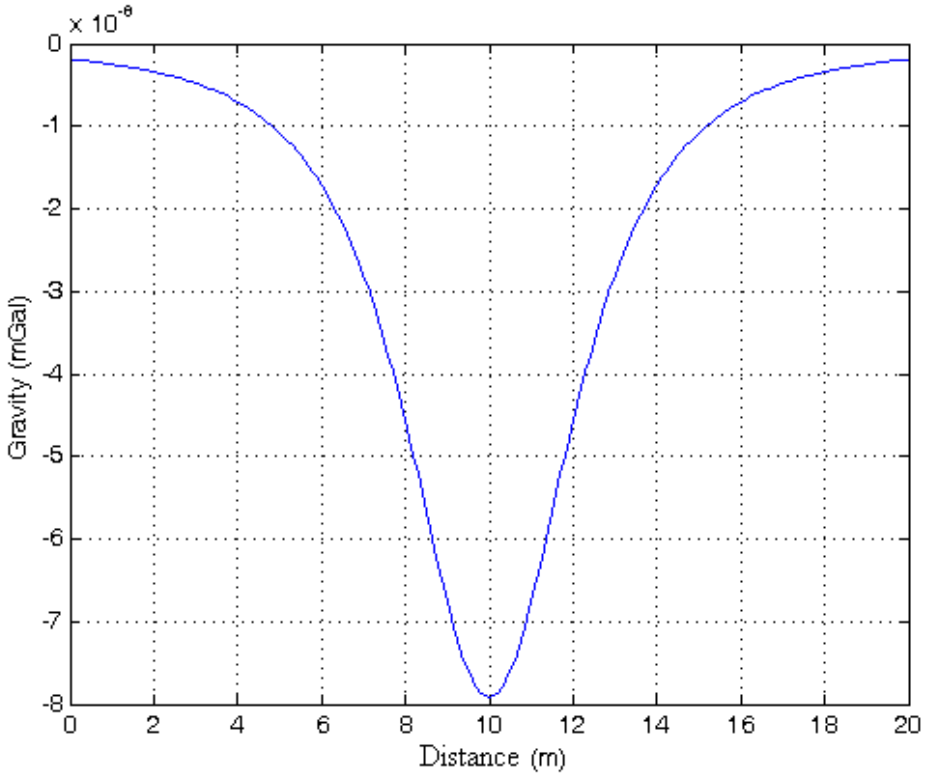

Figure 3.13: Residual gravity anomaly curve over cavity filled with pure air.

3.3.2 Model 2: Cavity filled with pure water

In this model, the cavity is filled with pure water with a density of 1000 kg/m^3, and the surrounding environment has a density of 2550 kg/m^3. Hence, there is a density contrast between the cavity and the surrounding limestone, causing a gravity anomaly of $g_{max} = -0.00004814\mu Gal$, this is shown in Figure 3.14.

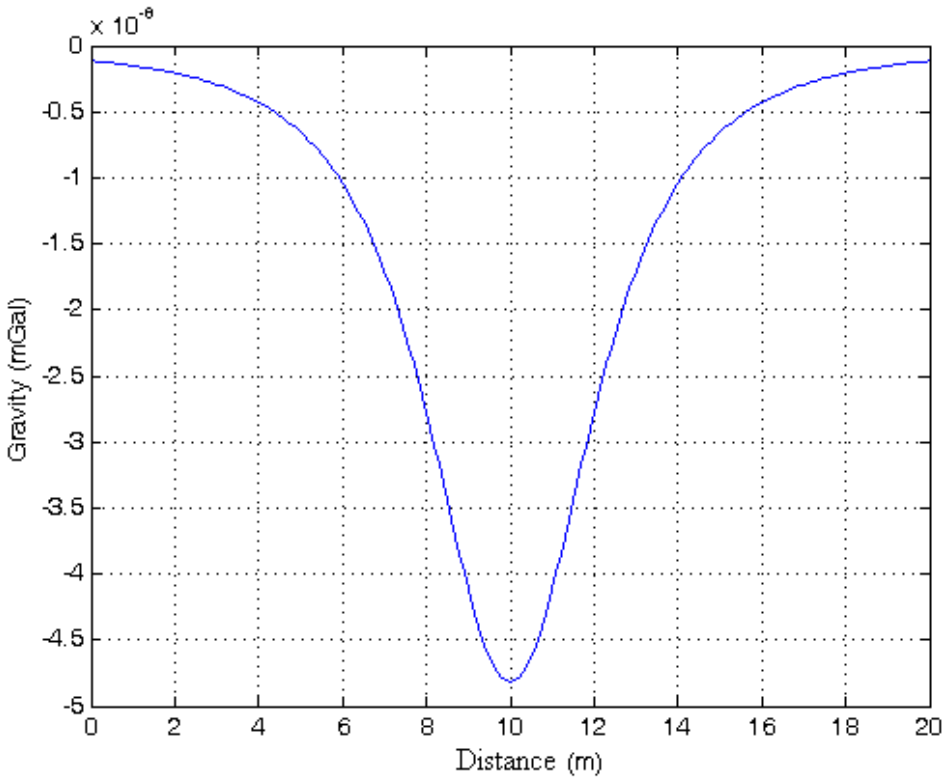

Figure 3.14: Residual gravity anomaly curve over cavity filled with pure water.

3.3.3 Model 3: Cavity filled with dry sand

In this model, the cavity is filled with dry sand with a density of 1855.3 kg/m^3. This density is calculated by using the porosity-density relationship (Eq. 2.7) with a porosity equal to 0.3, a water saturation equal to zero and the other values held constant. These factors are tabulated in Table 3.1. The maximum gravity anomaly due to this cavity material is equal to $g_{max} = -0.0000216\ \mu Gal$, as shown in Figure 3.15.

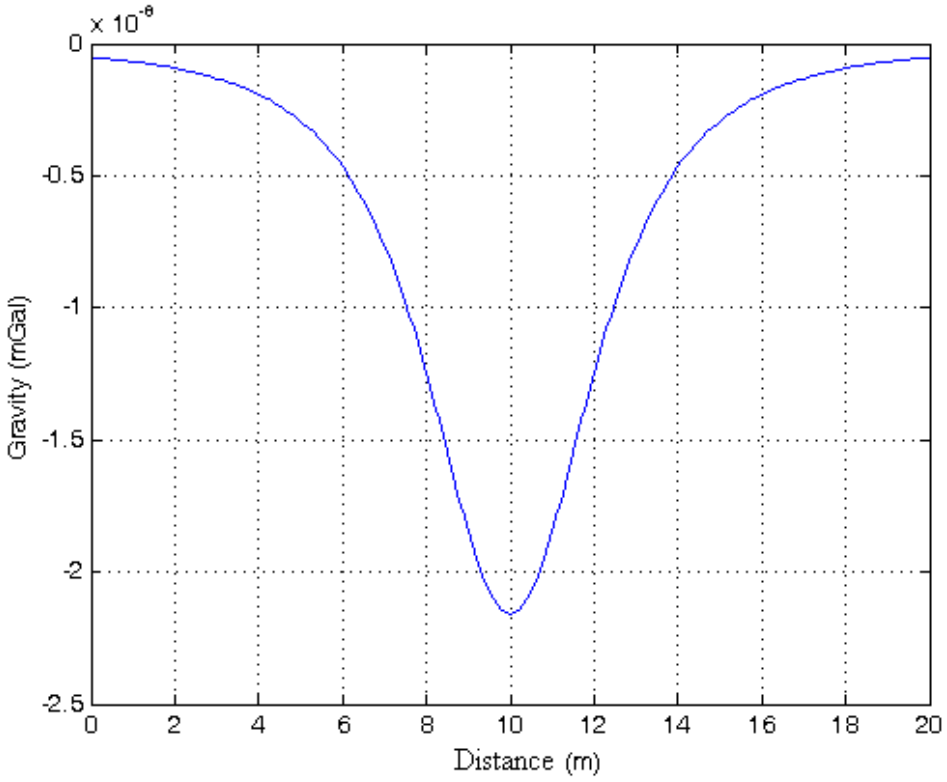

Figure 3.15: Residual gravity anomaly curve over cavity filled with dry sand.

3.3.4 Model 4: Cavity filled with partially saturated sand

In this model, the cavity is filled with partially saturated sand with a density of 2005.15 kg/m^3. This density is calculated by using porosity-density relationship (Eq. 2.7) with a porosity equal to 0.3, a water saturation equal to 0.5 and other values held constant. These factors are tabulated in Table 3.1. The maximum gravity anomaly due to this cavity material is equal to $g_{max} = -0.000017 \mu Gal$, as shown in Figure 3.16.

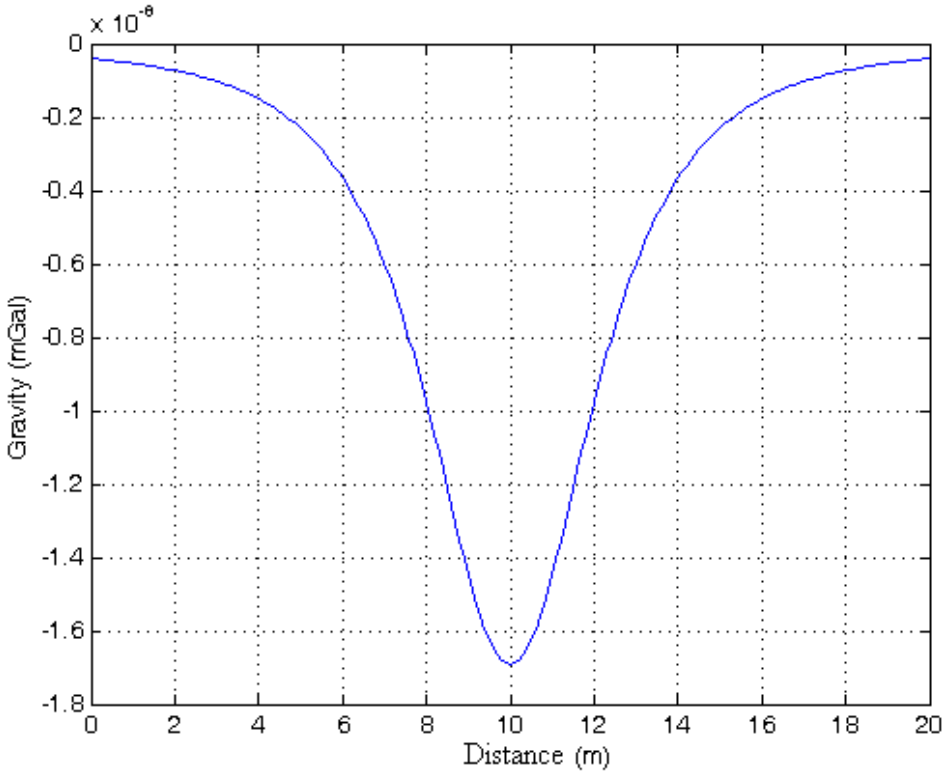

Figure 3.16: Residual gravity anomaly curve over cavity filled with partially saturated sand.

3.3.5 Model 5: Cavity filled with fully saturated sand

In this case, the cavity is filled with fully saturated sand, and the density of the cavity material is 2155 kg/m^3 because the porosity and water saturation were 0.3 and 1, respectively. Therefore, the maximum gravity anomaly value directly above the cavity is $g_{max} = -0.0000123\ \mu Gal$, as shown in Figure 3.17.

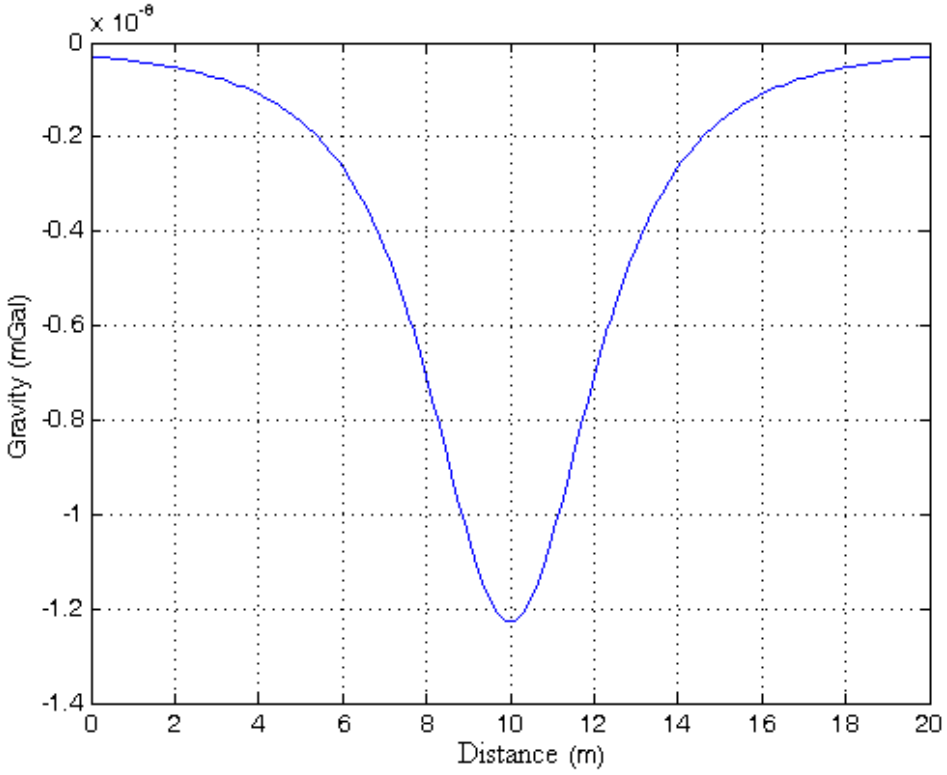

Figure 3.17: Residual gravity anomaly curve over cavity filled with fully saturated sand.

Finally, the extracted information from the radargrams and the Bouguer gravity anomaly curves for all synthetic models are summarized in table 3.2. That information is important for the joint inversion approach to estimate the porosity and water saturation in next chapter.

Models	Gravity anomaly (MicroGal)	X(1/2) (m)	Tc (ns)
Cavity filled with pure air	-0.0000792	2.3	63.56
Cavity filled with pure water	-0.0000481	2.3077	170.7
Cavity filled with dry sand	-0.0000216	2.3014	74.22
Cavity filled with partially saturated sand	-0.000017	2.3	89.33
Cavity filled with fully saturated sand	-0.0000123	2.31	104.4

Table 3.2: Extracted information from radargrams and Bouguer anomaly curves required for inversion.

Chapter 4

RESULTS AND DISCUSSION

4.1 Overview

This chapter summarizes the research carried out and the major findings of this thesis. In addition, a sensitivity analysis of the method is demonstrated.

4.2 Results

The total travel time (T_c) from the surface to the interface directly beneath the cavity is picked from radargram and the maximum gravity anomaly (g_{max}) directly above the cavity is deduced from the residual Bouguer gravity anomaly over the cavity. Both of these parameters are summarized in Table 4.1.

These two important parameters are used in the inversion of porosity and water saturation values using equations 2.28 and 2.29.

This approach was verified using the five different cases of cavity materials listed in Chapter 3. The results are displayed in the last four columns of Table 4.1, which represent the porosity and water saturation values inverted from the five cases using this new approach. It also shows the absolute percentage error of these values from the true values assumed in the generation of synthetic data by forward modeling.

In the first model, in which the cavity is filled with pure air, the assumed values for porosity and water saturation were 1 and zero, respectively, in the forward modeling. After I applied this approach through formulas 2.28 and 2.29, I obtained a porosity of 1.01587 and a water saturation value of 0.00206. Therefore, the absolute percentage error in this case was 1.6% and 0.21% for porosity and water saturation values, respectively.

In the second case, in which the cavity is filled with water, the values of the porosity and water saturation used in the forward modeling were 1 and 1, respectively. Therefore, the inverting process using formulas 2.28 and 2.29 resulted in a porosity of 1.00657 and a water saturation of 1.00753. The corresponding absolute percentage errors are 0.7% and 0.8% for porosity and water saturation, respectively.

In model 3, in which the cavity is filled with dry sand, the true value

of porosity was 0.3, and the water saturation was zero. Applying joint inversion approach to estimate porosity and water saturation, I obtained values of 0.304795 for porosity and 0.011623 for water saturation. The corresponding absolute percentage errors were 1.6% for porosity and 1.16% for water saturation.

In the same manner, the input parameters of porosity and water saturation in the forward modeling of a cavity filled with partially saturated sand are 0.3 and 0.5, respectively. The output results using equations 2.28 & 2.29 are 0.30229 for porosity and 0.48801 for water saturation, giving absolute percentage errors of 0.76% in porosity and 2.4% in water saturation.

Finally, for the case in which the cavity is filled with fully saturated sand, the input porosity and water saturation values are 0.3 and 1, respectively. The values from the joint inversion approach for this case are 0.29499 for porosity and 0.97493 for water saturation. The corresponding absolute percentage errors are 1.67% for porosity and 2.51% for water saturation.

All the results for porosity and water saturation from the different scenarios are acceptable and have high accuracy. For all cases, the error is always less than 2.51%. Moreover, for water saturation and porosity the highest errors are 2.51% and 1.67% and the lowest errors are 0.2% and 0.7%, respectively.

We observe that, in general, this new approach provides a reliable method to estimate porosity and water saturation for cavity-filling materials. The method commonly provides enough information to obtain a general view of the cavity's

contents, and this information could be used to characterize possible hazards associated with this cavity. This method could help engineers to estimate and calculate many geotechnical parameters that depend on these petrophysical parameters.

Cavity models	Input parameters $\varepsilon_g = 4.5$, $\varepsilon_w = 80$, $\varepsilon_a = 1$ $\rho_g = 2650(kg/m^3)$ $\rho_w = 1000(kg/m^3)$, $\rho_a = 1(kg/m^3)$					Output gravity data Picking from residual gravity curve		Output travel time from radargram Picking from synthetic GPR data		Output parameters			
												Absolute percentage error (%)	
	$\rho_b(kg/m^3)$	$v(m/ns)$	ϕ	S_w	ε_b	$g_z(\mu Gal)$	$x_{1/2}(m)$	$T_{top}(ns)$	$T_c(ns)$	ϕ	S_w	$\phi(\%)$	$S_w(\%)$
Cavity filled with pure air	1	0.2998	1	0	1	-0.0000792	2.3	34.22	63.56	1.01587	0.00206	1.6	0.21
Cavity filled with pure water	1000	0.033518	1	1	80	-0.0000481	2.3077	34.22	170.7	1.00657	1.00753	0.7	0.8
Cavity filled with dry sand	1855.3	0.168	0.3	0	3.18596	-0.0000216	2.3014	34.22	74.22	0.304795	0.01162	1.6	1.16
Cavity filled with partially saturated sand	2005.15	0.1007	0.3	0.5	8.8599	-0.000017	2.3	33.33	89.33	0.30229	0.48801	0.76	2.4
Cavity filled with fully saturated sand	2155	0.071924	0.3	1	17.374	-0.0000123	2.31	33.33	104.4	0.29499	0.97499	1.67	2.51
Limestone background	2550	0.12	0.3	0	6.25								
Shale bed rock	2420	0.09			11.111								

Table 4.1: The density and dielectric permittivity values used in forward modelling, synthetic gravity and GPR results and the values of porosity and water saturation calculated by joint inversion approach with errors.

4.3 Sensitivity Analysis

The porosity-density relationship expresses the bulk density of the materials in terms of fluids and matrix densities, whereas the CRIM describes the bulk permittivity of a composite material in terms of the dielectric permittivities of its constituent grains and fluids. In addition, the empirical constants in the CRIM and porosity-density relationship might be unknown or difficult to determine for a given survey area. Therefore, this section investigates the effects of using incorrect petrophysical parameters (i.e., density and dielectric permittivity of the grains or matrix) in the joint inversion approach. There is also a discussion of how incorrect values distort the porosity and water saturation values estimated by this new approach.

The main unknowns when using this new approach are the values of density and dielectric permittivity of the grains of the material within the cavity, which are then used to estimate the porosity and water saturation of the material. Therefore, to measure the sensitivity of this approach to incorrect density and permittivity values, I conduct a sensitivity analysis.

The changes in the porosity and water saturation values due to using incorrect matrix densities and dielectric permittivities were calculated for the cavity filled with materials through joint inversion approach of GPR and gravity data sets. Figures 4.1 and 4.2 show 3D plots of the absolute percentage errors in porosity and water saturation estimations as functions of different values of

matrix densities and dielectric permittivities.

The range of the matrix density is between 2100 kg/m^3 and 3000 kg/m^3, which includes most shallow rocks, while the true value in the tested models was 2650 kg/m^3. The range of the matrix dielectric permittivity varies from 2.5 to 10, which represents most sediments, while the true value for the tested models was 4.5.

4.3.1 Effects of incorrect grain density and permittivity on porosity estimation

Figure 4.1 shows a 3D plot of the distribution of absolute percentage error in estimated porosity associated with various values of matrix density and dielectric permittivity. The absolute percentage errors increase with deviation from the true values of ρ_g and ϵ_g. The smallest absolute percentage error in porosity values occurs between a matrix density of 2600 kg/m^3 and 2800 kg/m^3 along the density axis. Therefore, the smallest error lies around the true value used in the inversion operation. The sensitivity plot shows that the inverted porosity by this new approach is more sensitive to the matrix density than dielectric permittivity. Thus, to get a good estimation of porosity with this approach, one should be careful when selecting the matrix density.

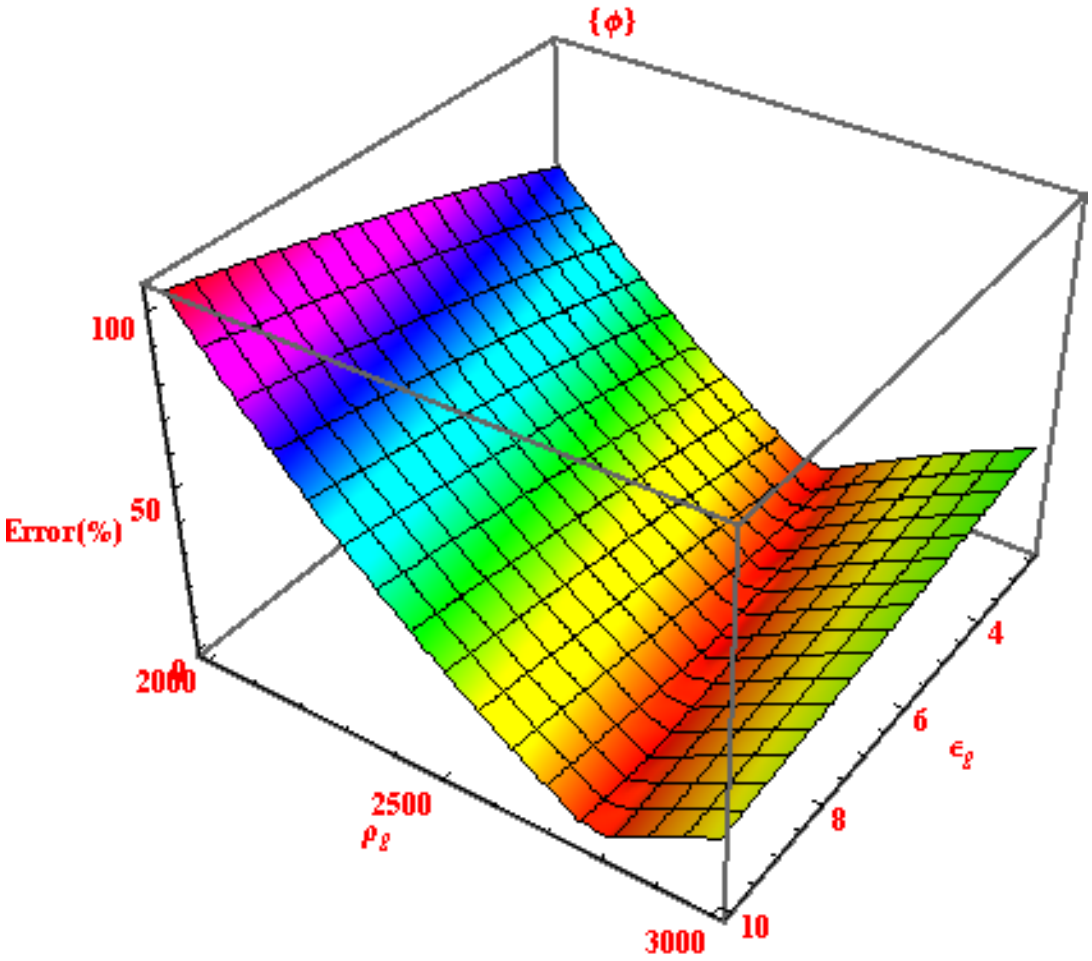

Figure 4.1: 3D plot of the absolute percentage error in porosity as a function of matrix density and dielectric permittivity.

4.3.2 Effects of incorrect grain density and permittivity on water saturation estimation

Figure 4.2 shows a 3D plot of absolute percentage errors in water saturation associated with various values of matrix density and dielectric permittivity. It is clear that the absolute percentage error increases gradually with increasing

matrix dielectric permittivity and decreasing matrix density from the true values of ρ_g and ϵ_g. The smallest absolute percentage error in water saturation occurs between a matrix dielectric permittivity of 3.5 and 5 along permittivity axis. Therefore, the smallest error lies around the true value used in the inversion operation which is 4.5. In addition, the sensitivity plot shows that the inverted water saturation by this new approach is more sensitive to errors in matrix dielectric permittivity than matrix density. Thus, to get a good estimation of water saturation with this approach, one should be careful when selecting the matrix dielectric permittivity.

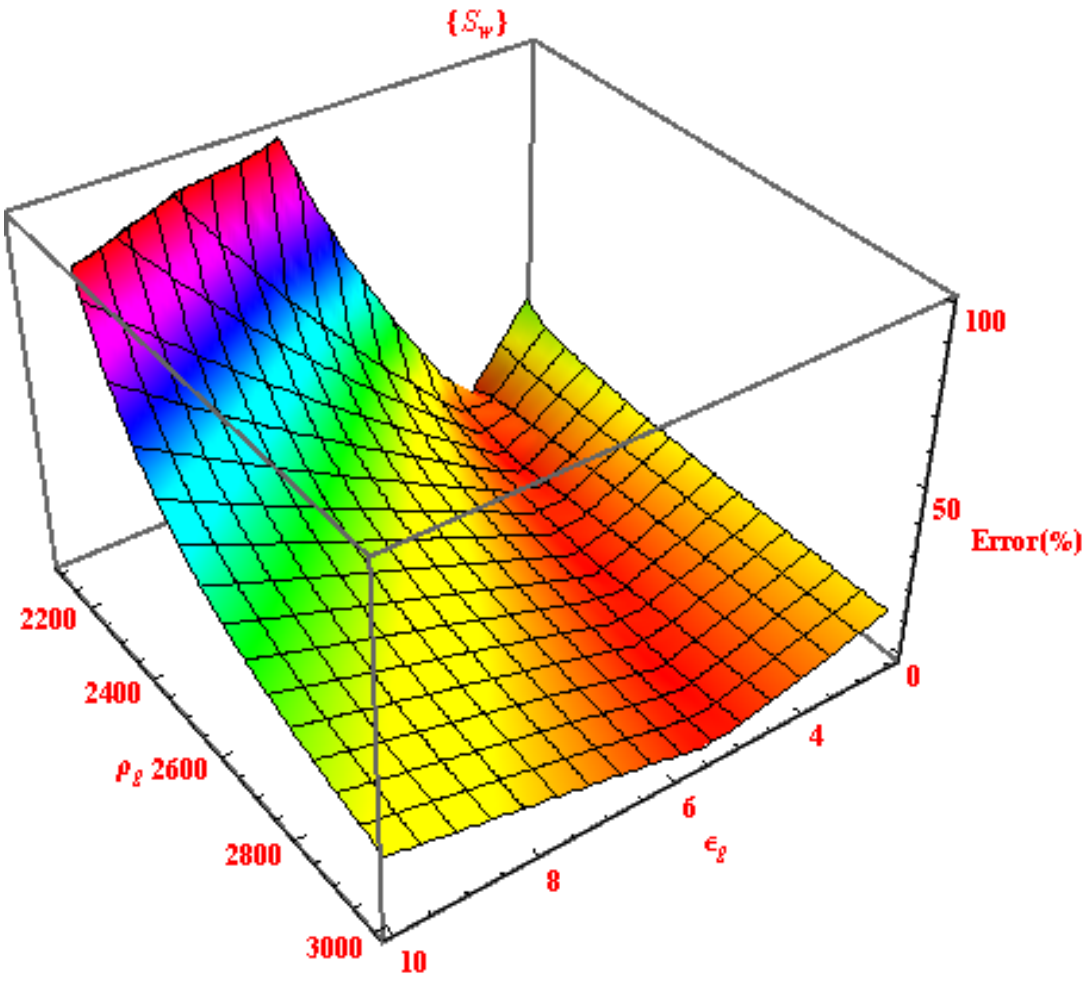

Figure 4.2: 3D plot of absolute percentage error in water saturation of matrix density and dielectric permittivity.

Chapter 5

CONCLUSIONS AND RECOMMENDATIONS

5.1 Conclusions

In this study, the development and characterization of a new GPR and gravity joint inversion has been presented. This approach is validated to estimate porosity and water saturation for the material inside a cavity through synthetic data. It demonstrates the ability of the joint inversion approach to provide an accurate value of porosity and water saturation for cavity filling materials.

I described the petrophysical models I used to link bulk dielectric permittivity and bulk density with porosity and water saturation parameters. These

factors are used in a quantitative joint inversion approach to estimate porosity and water saturation from GPR and gravity measurements.

The GPR synthetic data is computed using a 2D split-step algorithm which requires the solution of Maxwell's equations in the frequency domain. This algorithm is implemented via the MATGPR software. Additionally, the synthetic gravity anomaly curves are generated using MATLAB functions through analytical expressions for an earth model composed of a 2D horizontal slab which represents the background rock and a spherical body that represents the cavity.

The basic cavity model used in this study consists of horizontal and vertical dimensions of 20 m and 10 m, respectively with a horizontal interface at depth of 5 m which separates an upper limestone bed from a lower shale bedrock. In addition, there is a spherical cavity with 1 m radius with its center located at 3 m in depth and 10 m horizontal distance.

The basic outcomes of this thesis are equations 2.28 and 2.29, which can be used to determine the porosity and water saturation of cavity-filling materials through the joint inversion of GPR and gravity data sets. This approach was successfully applied to synthetic GPR and gravity data for various spherical cavity materials. More specifically, five synthetic models have been tested on this approach. The materials within cavity are composed of air, water, dry sand, partially saturated sand or fully saturated sand.

This study also showed generally the high accuracy results for all cases.

The error was always less than 2.51%. Moreover, for water saturation and porosity the highest errors are 2.51% and 1.67%, respectively; whereas the lowest errors are 0.2% and 0.7%, respectively.

In general, this thesis has contributed to the characterization of the cavity phenomena, covering the detection of the porosity and water saturation of cavity material. The proposed method is efficient in calculating the porosity and water saturation for a spherical cavity shape. The developed methodology provides accurate results when applied to simulated datasets. However, the result produced by the joint inversion is sensitive to incorrect matrix density and dielectric permittivity values used in inverting porosity and water saturation parameters for materials inside the cavity. Moreover, if this approach is applied to real data, this might be a challenging task. If no matrix permittivity and density data are available, this approach might result in high errors in the estimated parameters. One has to be careful in collecting field data and in dealing with the correction of microgravity anomalies due to the effects of topographic variation and precision of the gravimeter when detecting the very small anomalies associated with cavities. Thus, for real data all of these circumstances must be constrained to obtain a good result by using this approach.

With other model, one can formulate a set of equations for the selected model, such as irregular shape, horizontal sheet or any other shape. Consequently, porosity and water saturation can be determined with the joint inversion approach of GPR and gravity data sets. Further investigation in the future may be performed to extend this approach to address an irregularly shaped

cavity or a set of multiple cavities.

5.2 Recommendations

The proposed GPR and gravity joint inversion approach could be extended to estimate porosity and water saturation for non-spherical cavity such as irregular shapes. Additionally, instead of CRIM, another rock-physics model can be used such as Topp's equation and Bruggeman-Hanai-Sen (BHS) model.

The methodology developed here is not only restricted to GPR and gravity techniques but it also can be extended to include other geophysical tools such as seismic and electrical resistivity. In addition, this approach can be used with three or more techniques that are sensitive to the same subsurface petrophysical quantities. Thus, any group of geophysical data sets that have a common petrophysical link can be inverted using this approach.

Bibliography

Al-Shuhail, A.A. , Hariri, M.M. and Makkawi, M.H. 2004: Using ground penetrating radar to delineate fractures in the Rus Formation, Dammam Dome, Eastern Saudi Arabia. International Geology Review, Vol.46, Iss. 1, P. 91-96.

Annan, A. P. and S. W. Cosway 1992: Ground penetrating radar survey design, in proceeding of the Symposium on the Application of Geophysics to Engineering and Environmental Problems SAGEEP. 92, Chicago, 329-351.

Benson, A.K. 1995: Applications of ground penetrating radar in assessing some geological hazards: examples of groundwater contamination, faults, cavities. Journal of Applied Geophysics, vol.33, p. 177-193.

Bishop, I., Styles P., Emsley S. J., Ferguson N. S., 1997: The detection of cavities using the microgravity technique: case histories from mining and

karstic environments. Modern Geophysics in Engineering Geology, Geological Society, Engineering Geology Special Publication, vol.12, p. 153-166.

Bitri, A. and Grandjean, G., 1998: Frequency wavenumber modelling and migration of 2D GPR data in moderately heterogeneous dispersive media, Geophysical Prospecting, 46, 287-301.

Butler, D.K., 1984a: Interval gravity-gradient determination concepts. Geophysics, 49/ 6, p. 828-832.

Butler, D. K., 1984b: Microgravimetric and gravity gradient techniques for detection of subsurface cavities. Geophysics, vol. 49/7, p.1084-1096.

Chalikakis, K., Plagnes, V., Guerin, R., Valois, R. and Bosch, F.P.2011: Contribution of geophysical methods to karst-system exploration: an overview. Hydrogeology Journal, vol. 19, p. 1169-1180.

Chamberlain, A.T., Sellers, W., Proctor, C. and Coard, R. 2000: Cave Detection in Limestone using Ground Penetrating Radar. Journal of Archaeological Science, vol. 27, p. 957-964.

Colley, G.C., 1963: The detection of caves by gravity measurements. Geophysical Prospecting, vol. 11/ 1, p. 1-9.

Conyers, L.B., 2004: Ground-Penetrating Radar for Archaeology. Walnut Creek, CA ; Oxford: AltaMira Press.

Daniels, D.J., 2004: Ground Penetrating Radar. 2nd ed, London, Institution of Electrical Engineers. 726.

Davis, J. L. and Annan, A. P. 1989: Ground-penetrating radar for high-resolution mapping of soil and rock stratigraphy. Geophysical Prospecting, 37, 531-551.

Do, J., 2003: Ground Penetrating Radar. Villanova University: Pennsylvania. p. 5.

Dojack, L., 2012: Ground Penetrating Radar Theory, Data Collection, Processing and Interpretation: A guide for Archaeologists, M. A. and S. Daniel, Editors. University of British Columbia: Vancouver. p. 94.

Fiore, V.Di., Angelino, A., Passaro, S. and Bonanno, A. 2011: High resolution seismic reflection methods to detect near surface cavities: a case study in the Neapolitan area, Italy. Journal of Cave and Karst Studies, v. 75/ 1, p. 51-59.

Gambetta, M., Armadillo, E., Carmisciano, C., Stefanelli, P., Cocchi, L. and Tontini, F.C. 2011: Determining geophysical properties of a

near surface cave through integrated microgravity vertical gradient and electrical resistivity tomography measurements. Journal of Cave and Karst Studies, vol. 73/1, p. 11-15.

Grealy, M., 2006: Resolution of Ground-Penetrating Radar Reflections at Differing Frequencies. Archaeological Prospection. 13(2): p. 142-146.

Hajian, A., Zomorrodian, H., Styles, P., Greco, F. and Lucas, C., 2012: Depth estimation of cavities from microgravity data using a new approach: the local linear model tree (LOLIMOT). Near Surface Geophysics,vol. 10, p. 221-234.

Luo, Y. and G.Y. Fang, 2005: GPR Clutter Reduction and Buried Target Detection by Improved Kalman Filter Technique. Proceedings of 2005 International Conference on Machine Learning and Cybernetics, Vols 1-9, p. 5432-5436.

Metwaly, M. and AlFouzan, F. 2013: Application of 2-D geoelectrical resistivity tomography for subsurface cavity detection in the eastern part of Saudi Arabia. Geoscience Frontiers, vol.4, p.469-476.

Mochales, T., Casas, A.M., Pueyo, E.L., Pueyo, O., Roman, M.T. Pocovi, A. Soriano M.A. & Anson, D. 2008: Detection of u8nderground

cavities by combining gravity, magnetic and ground penetrating radar surveys: a case study from the Zaragoza area, NE Spain. Environ Geol 53: p 1067-1077.

Nettleton, L.L. 1942: Gravity and magnetic calculations. Geophysics, 7, 293-310.

Nettleton, L.L. 1940: Geophysical Prospecting for Oil. McGraw-Hill.

Nettleton, L.L. 1976: Gravity and Magnetics in Oil Prospecting. McGraw-Hill.

Olhoeft, G.R., 2000: Maximizing the Information Return from Ground Penetrating Radar: J. Applied Geophysics, v. 43, no. 2-4, pp. 175-187.

Pánisová, J., Pasteka, R. 2009: The use of microgravity technique in archaeology: A case study from the St. Nicolas Church in Pukanec, Slovakia. Contributions to Geophysics and Geodesy vol. 39/3, p. 237-254.

Pernod, P., Piwakowski, B., Delannoy, B. and Tricot, J.C. 1989: Detection of shallow underground cavities by seismic methods: physical modelling approach. Acoustical Imaging, vol. 17, p 705-713.

Putiska, R., Nikolaj, M., Dostal, I., and Kusnirak, D. 2012: Deter-

mination of cavities using electrical resistivity tomography. Contributions to Geophysics and Geodesy, vol. 42/2, pp. 201-211.

Reynolds, J.M. 1997: An introduction to applied and environmental geophysics. John Wiley & Sons Ltd., West Sussex, England, p. 800.

Russell, B., Hedlin, K., Hilterman, F. and Lines, L., 2003, Fluid-property discrimination with AVO: A Biot-Gassmann perspective: Geophysics,68, 29-39.

Scheele, M., 2011: Techniques for Clutter Reduction for GPR Images, in Department of Electronic and Computer Engineering. University of Portsmouth: Portsmouth. p. 41.

Styles, P., McGrath, R., Thomas, E. and Cassidy, N.J., 2005: The use of microgravity for cavity characterization in karstic terrains. Quarterly Journal of Engineering Geology and Hydrogeology, vol. 38, p. 155-169.

Telford, W.M., Geldart, L.P., and Sheriff, R.E. 1990: Applied Geophysics. Cambridge University Press, Cambridge.

Tzanis, A., 2010: matGPR Release 2: A freeware MATLAB package for the analysis & interpretation of common and single offset GPR data,

FastTimes, 15 (1), 17 - 43.

Xue, G., Song, J., Xian, Y., 2004: Detecting shallow caverns in China using TEM. The Leading Edge 23 (7).

Vitae

- Fathi Mohammed Saeed Abdullah.
- Born in Taiz, Yemen on Januray 01, 1981.
- Graduated from high school in 2000.
- Received Bachelor of Science (BSc) degree in Geophysic (batch 2005-2006) from Taiz University , Taiz, Yemen in 2006.
- Appointed as a graduate assistant at Taiz University, College of Science in 2008, and I am still working there as a faculty member.
- Received a scholarship from the Ministry of Higher Education and Taiz University to study MS degree at KFUPM in 2010.
- **Participation:** 2nd SEG Middle East Geoscience Student Symposium, Muscat, Oman, (26-29) April 2014.

- **Present Address:** Department of Earth Science, King Fahd University of Petroleum and Minerals, Dhahran, Saudi Arabia.
- **E-mail Address:** g201002180@kfupm.edu.sa.
- **Permanent Address:** Department of Geology, Taiz University, Taiz, Yemen.
- **E-mail Address:** fms_202@yahoo.com.